View Online / Journal Homepage
Dynamic Article Links

Lab on a Chip

Cite this: DOI: 10.1039/c2lc40787f

www.rsc.org/loc

PAPER

Full range physiological mass transport control in 3D tissue cultures†

Yu-Hsiang Hsu,[af] Monica L. Moya,[af] Parinaz Abiri,[a] Christopher C.W. Hughes,‡[abf] Steven C. George‡[acdf] and Abraham P. Lee‡*[ae]

Received 11th July 2012, Accepted 9th October 2012
DOI: 10.1039/c2lc40787f

We report the first demonstration of a microfluidic platform that captures the full physiological range of mass transport in 3-D tissue culture. The basis of our method used long microfluidic channels connected to both sides of a central microtissue chamber at different downstream positions to control the mass transport distribution within the chamber. Precise control of the Péclet number (Pe), defined as the ratio of convective to diffusive transport, over nearly five orders of magnitude (0.0056 to 160) was achieved. The platform was used to systematically investigate the role of physiological mass transport on vasculogenesis. We demonstrate, for the first time, that vasculogenesis can be independently stimulated by interstitial flow (Pe $>$ 10) or hypoxic conditions (Pe $<$ 0.1), and not by the intermediate state (normal living tissue). This simple platform can be applied to physiological and biological studies of 3D living tissue followed by pathological disease studies, such as cancer research and drug screening.

Introduction

A living tissue is three-dimensional (3-D) and is comprised of cells and extracellular matrix (ECM) that interact mechanically and biochemically.[1,2] To understand cellular behavior in 3-D microenvironments it is critical to precisely mimic the chemical and mechanical environment of a living tissue.[3] This requires the ability to precisely control mass transport over the entire physiological range in order to recapitulate the processes regulating tissue growth and response to chemical (*e.g.* growth factors) and mechanical (*e.g.* shear stress) stimuli. Interstitial mass transport and flow contributes to tissue development, survival, and function by impacting ECM remodeling,[4] mechanotransduction,[5–7] and cellular migration.[8,9] The role of mass transport has been studied extensively to understand angiogenesis,[10–20] vasculogenesis,[10,17,21,22] lymphangiogenesis,[11,12,15,21] and tumorigenesis.[23–25] Growth factors and morphogens form gradients in tissues as they diffuse away from their source. For example, local hypoxia induces Vascular Endothelial Growth Factor (VEGF) expression by interstitial fibroblasts. The magnitude of these gradients is affected by concentration, affinity for matrix, and flow, and can dramatically impact cellular responses such as angiogenesis by endothelial cells (ECs).[10,16] Interstitial flows that approximate those seen *in vivo* (0.1 to 1 μm s^{-1} in normal adult tissue) can modulate *in vitro* vessel formation.[12,13,16,17,19,21] In particular, interstitial flow can stimulate vasculogenesis and influence vessel formation synergistically with cell-secreted morphogens in asymmetric concentration distributions.[16] Indeed, numerical simulations demonstrate that interstitial flow in the range of 0.1–6 μm s^{-1} can redistribute morphogen gradients.[21] The experimental designs in these studies has been limited to that observed in healthy tissues, where new blood vessel growth is generally absence or negligible. In contrast disease or altered physiological states (*e.g.*, tumor, wound healing, exercise) can significantly alter metabolic demand and interstitial flow, and are associated with new blood vessel growth. The impact of convection and diffusion over the entire range encountered in both disease and healthy tissue is not known.

Current approaches to control constant interstitial flow in a microchamber use one of the following: media reservoirs of different heights to create hydrostatic pressures, passive pumps driven by surface tension, or external circulation systems with active pumps.[13,17,19,21] Passive pumps usually require frequent adjustment of media volume, and active pumps are bulky and not amendable for scale up. To systematically study the role of mass transport in a 3-D physiological microenvironment, we developed a universal microfluidic platform that can easily and precisely manipulate convective and diffusive mass transport over a large range, and thus can model healthy and diseases tissue with an unprecedented level of control. The basis of our

[a]*Department of Biomedical Engineering, University of California, Irvine, CA 92697, USA. E-mail: aplee@uci.edu; Fax: +1-(949) 824-1727; Tel: +1-(949) 824-9691*
[b]*Department of Molecular Biology and Biochemistry, University of California, Irvine, CA 92697, USA*
[c]*Department of Chemical Engineering and Materials Science, University of California, Irvine, CA 92697, USA*
[d]*Department of Medicine, University of California, Irvine, CA 92697, USA*
[e]*Department of Mechanical and Aerospace Engineering, University of California, Irvine, CA 92697, USA*
[f]*Edwards Lifesciences Center for Advanced Cardiovascular Technology, University of California, Irvine, CA 92697, USA*
† Electronic supplementary information (ESI) available. See DOI: 10.1039/c2lc40787f
‡ These authors contributed equally to this work

method is a long microfluidic channel that distributes the flow and the resulting mass transport precisely across a microtissue chamber. This is the first method that can replicate the full physiological range of mass transport in an *in vitro* 3-D tissue culture. The potential impact of this platform is three-fold. First, the mass transport can be manipulated freely, precisely and quantitatively. Second, the physiological environment can be fine tuned for developing a targeted living tissue with specified *in vivo* conditions. Third, the developed microtissue can be used as an *in vitro* model to study disease formation.

In this paper, vasculogenesis is chosen as the biological endpoint to demonstrate the importance of controlling mass transport in a 3D tissue model. With precise control of the Péclet number, our experimental data clearly show for the first time that vasculogenesis can be independently stimulated by interstitial flow or hypoxic conditions but not the intermediate state (normal living tissue). This result exemplifies the biological usefulness of this new method. The presented platform is universal and can be applied to a broad range of living 3D tissue studies in health and in disease, including cancer research and drug screening.

Design of microfluidic network

Our design employs a long microchannel to manipulate the pressure over a wide range and, thus the mass transport within the microphysiological environment. This concept is most easily understood using an analogy between the microfluidic network and an electric circuit.[26] With fully developed laminar flow, a long microchannel is effectively a series of hydraulic resistors connected end to end. The length (resistance) and flow inside (current) of each resistor determines the pressure drop (voltage). The overall pressure drop establishes the pressure distribution and the resultant mass transport inside the microtissue chamber. The pressure drop is linear between the high entrance pressure (black; P_H) and the low exit pressure (white; P_L) (Fig. 1A). By connecting two sides of a microtissue chamber through multiple communication pores of the long microchannel, the pressure drop in the microchannel determines the pressure distribution inside the tissue chamber. A higher pressure gradient can be created with a longer segment of the microchannel connecting the two sides (Fig. 1A, left microtissue chamber), and a lower pressure drop can also be created with a shorter segment (Fig. 1A, right microtissue chamber).

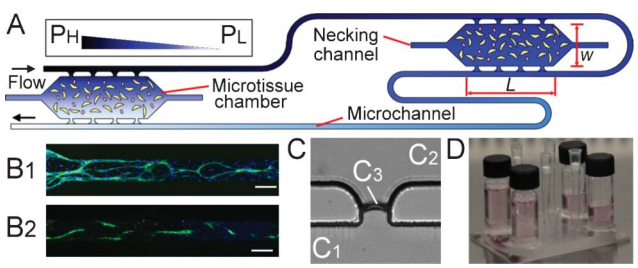

Fig. 1 (A) Schematic illustrating the use of a long microchannel to control the physiological environment in a microtissue chamber. The long microfluidic channel creates a large range of pressures. The microtissue compartment can be positioned at different locations along the microfluidic channel resulting in either a large (left chamber) or small (right chamber) pressure drop across the tissue and thus a large or small convective flow. Capillary morphogenesis in the necking channel (B_1) adjacent to microchamber and 3–4 mm away (B_2) is suppressed. (C) The capillary burst valve design for the communication pore, (D) one of the microfabricated microplatform and media reservoirs.

We designed four microfluidic platforms to systematically study the influence of convection and diffusion on vasculogenesis, and quantified the relative magnitude of convection to diffusion using the Péclet number (Pe and supplement). The contributions of convection and diffusion were verified by finite element simulations, and measuring the mass transport of fluorescein isothiocyanate FITC-dextran flowing into the microtissue chamber from the long microchannel. The total length of the long microchannel (510 to 780 mm long and 100 μm on each side, supplement) is more than 130 times longer than the microtissue chamber (L = 4 mm, W = 1 mm, and 100 μm in depth) to create a large hydraulic resistance. The small communication pores (100 μm by 30 μm) and porous matrix of the 3-D cell construct in the microtissue chamber provides a hydraulic resistance more than 50 times larger than the total resistance of the microchannel. As a result, the microtissue chamber has a negligible effect on the linear pressure drop of the microchannel. The microchamber is tapered horizontally at each end to necking channels 200 μm in width, 7 mm in length and 100 μm in depth. The tapered channels provides a symmetric geometry for balancing the contractile forces generated by the microtissue. The necking channels provided a means to load the liquid microtissue construct by pipetting. More importantly, these two necking channels significantly minimized the influence of vasculogenic stimuli from the cell suspension remaining in the necking channels and pipette tips (Fig. 1B1: adjacent to microchamber, 1B2: 3 to 4 mm away from the microchamber). This design ensures that the physiological environment is controlled predominantly by the flow distribution from the communication pores (see below).

The microtissue construct is created by loading a fibrin gel seeded with normal human fibroblasts (NHLFs) and endothelial colony forming cell-derived endothelial cells (ECFC-ECs)[27] in the microtissue chamber. The microplatform loaded with cell construct is incubated under 5% oxygen tension to mimic *in vivo* normoxia. The NHLFs served as the stromal cells, which are required for vasculogenesis and also as structural support of the microvessels.[28] To prevent fibrin gel leakage, a capillary burst valve is applied to the design of the communication pores.[29] Fig. 1C shows the function of the capillary burst valve, where the communication pore has smooth curvatures from the microchamber (C_1) to the microchannel (C_2) on two sides. When the fibrin gel flows out of the microchannel along these curved communication pores, the surface tension of the leading edge (C_3) will gradually increase and eventually equal and oppose the driving hydrostatic pressure. At this point, the fibrin gel will stop flowing, and thus does not enter the microfluidic channel. Finally, a near constant pressure drop in the long microchannel is maintained by using two media reservoirs with a large cross-sectional area (12.5 mm in diameter) and the high hydraulic resistance of the long microchannel (Fig. 1D and supplement). The maximum variation of the driving pressure is 20 μm H_2O h^{-1}.

Materials and method

A Cell culture

Endothelial colony forming cell-derived endothelial cells (ECFC-ECs) were isolated from cord blood as previously described[29] and expanded on gelatin-coated flasks in endothelial growth medium-2 (EGM-2, Lonza). Normal lung human fibroblast (NHLFs) purchased from Lonza were cultured in fibroblast growth media (Lonza). NHLFs (used at passage 3–5) and ECFC-derived ECs (used at passages 4–7) were both grown in a 37 °C/5% CO_2/20% O_2 incubator in 100% humidified air.

B Microtissue construct

The microtissue construct (Fig. 2) was created by loading a fibrin gel (10 mg ml^{-1}, A_1) seeded with NHLFs (A_2) and ECFC-ECs (A_3)[27] in a microchamber (volume 0.4 mm^3). The length (L), width (W), and depth (D) of the microchamber were 4, 1, and 0.1 mm, respectively. To prepare cell-matrix solution, bovine fibrinogen (Sigma-Aldrich, St. Louis, MO) was dissolved in DPBS to a final concentration of 10 mg ml^{-1}. NHLFs and ECs were suspended in the fibrinogen solution at a ratio of 2 : 1 to make a final cell density of 7.5 × 10^6 cells mL^{-1} total solution. The fibrinogen-cell solution was mixed with thrombin (50 U ml^{-1}) for a final concentration of 3 U ml^{-1} and quickly pipetted into the microchamber through a necking channel where it was allowed to fully polymerize. Fully supplemented cell culture medium was flowed into the side channels, and a microfluidic jumper (Fig. S1, a silicone tube that interconnects channel inlets) was then installed to complete connection. 20% oxygen tension was maintained for first 12 h, and then the fully supplemented media was replaced by EGM-2 without VEGF and bFGF. The levels of media in two reservoirs were leveled to maintain the desired pressure drop (ΔP), and the microfluidic platform was placed in a 5% O_2 incubator for 9 days. Media was levelled in the media reservoirs every other day. After 9 days, the microtissues were fixed and stained with CD31 antibody and DAPI for visualizing the vessel network and nuclei, respectively. Each physiological condition was repeated 3 to 5 times except only two for the highest interstitial flow conditions.

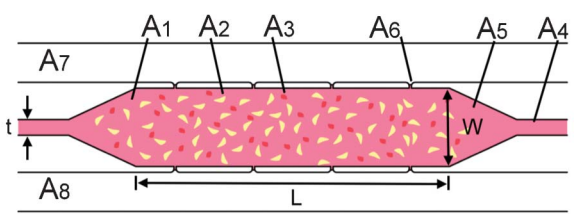

Fig. 2 Conceptual illustrations of the 3D microfluidic tissue model with 8 communication pores, where cell construct is formed by fibrin gel (A1) seeded with NHLFs (A2) and ECs (A3) and loaded through necking channel (A4) and wedge-shaped channel (A5). The physiological conditions are controlled by the magnitude of pressure facing into different communication pores (A6) along the microtissue through the fluidic side channels (A7–A8).

C Assessment of hypoxia

To assess the level of hypoxia in the microplatforms, cell constructs were treated with hypoxyprobe™-1 (pimonidazole hydrochloride) (HPI, Inc), and a 10 mm H_2O pressure drop were applied. After 1.5-day culture, 500 μM hypoxyprobe-1 were added to both media reservoirs of the long side channel without changing the media. The hypoxyprobe-1 flowed into the cell constructs through communication pores by convective and diffusive mass transport designed for each platform. Cell constructs were incubated for 36 h and then fixed and stained with 15 μg mL^{-1} FITC conjugated mouse monoclonal antibody IgG1 against hypoxyprobe-1 for 72 h followed by Alexa Flour 448 Goat anti-mouse secondary antibody for another 72 h. PDMS is highly permeable to oxygen (similar to that of water). Thus, the thickness of the top PDMS layer was made >8 mm to minimize the diffusion of oxygen from the incubator through the PDMS platform.[30] The thicker layer increases the diffusional resistance and thus the flux of oxygen. The bottom 1 mm thick PDMS was bonded to an oxygen impermeable glass slide. With this design, oxygen enters the microtissue primarily by convection and diffusion through the pores in the side channels. The control hypoxic condition was created using the microplatform with 16 communication pores and high transverse interstitial flow in a 1% O_2 incubator.

D Verification of mass transport

The contributions of convection and diffusion were verified both by finite element simulations and placing fluorescein isothiocyanate FITC-dextran (Sigma Aldrich, 70 kDa MW) into the high pressure side of the microfluidic channel at ΔP = 15 mm H_2O on day-1 without cells. The pattern of dextran flowing into the microchamber was acquired through real-time fluorescence imaging. The turnover time (T) was defined as the total time to fill the whole microchamber with dextran. The experimental results were compared to simulated results, and the dominant mass transport mechanism identified for each experiment. The velocity of convective or diffusive mass transport was calculated and represented by Va ± nVa, where Va is the spatial averaged velocity and n is a constant determining the velocity range controlled by necking channels. The averaged velocity Va was a spatial average of the velocity adjacent to communication pores and wedge-shaped channels. The Pe number of each condition was then calculated by using Va and compared to the microvessel network after the 9 day culture period (supplement).

E Finite element simulation

COMSOL Multiphysics® 3.5a was used to perform finite-element simulations of the mass transport induced in each microfluidic platform. 3-D microfluidic models were constructed and solved by a three-dimensional steady analysis of the incompressible Navier–Stokes equation. No-slip boundary condition was used for all surfaces except fluidic entrance and exit. Simulated pressure and velocity fields were used to interpret the magnitude and pattern of convection and diffusion. The initial condition of dextran was set to 1.0 mol m^{-3} at the entrance of the side channel. The dextran diffusion coefficient was 7 × 10^{-11} m^2 s^{-1}, the dynamic viscosity and density of water were 0.748

mPa s and 1 kg m^{-3}. The porosity and permeability of fibrin gel were adjusted to find the closest fit to experimental data and were 0.99 and 1.5 × 10^{-13} m^2 following the Brinkman equation.[16]

F Microfabrication of the PDMS microfluidic platform

A Si wafer was first cleaned with RCA-1 and 2% HF (Hydrofluoric acid) dip followed by spinning a 100 μm thick SU-8 100 (Micro Chem) layer. A single mask photolithography process then defined the microchamber, communication pores, and the long side channel. After silanizing with trichlorosilane ($C_8H_4Cl_3F_{13}Si$), a 10-to-1 ratio of polydimethylsiloxane (PDMS) prepolymer and curing agent (Dow Corning) was cast on the SU-8 mold to create a thick PDMS layer and then plasma bonded to a 1mm thick PDMS sheet. A 1 mm thick glass slide was then plasma bonded to the bottom of 1mm thick PDMS sheet. Two glass vials with the bottom removed were then glued to the entrance and exit of the long side channel with 10-to-1 ratio PDMS mixture and then cured in a 85 °C oven. The complete device was then sterilized at 121 °C for 20 min (Fig. 1D).

Results

A Experimental design

To simulate the full range of physiological cues for vasculogenesis, including hypoxia and interstitial flow, we created model platforms with a total of 8 (four on each side) and 16 (eight on each side) communication pores to control nutrient supply and the patterning of interstitial flow. We varied the total pressure drop (ΔP) across the microchannels by varying the height of fluid in the two media reservoirs of all four designs. Rather than a continuous spectrum of Pe, we chose ΔP to create very low Pe conditions (Pe < 0.1), intermediate (0.1 < Pe < 10), and very high (Pe > 10). The experimental and simulation results of the model with 8 communication pores are discussed here. The results with 16 communication pores can be found in the supplementary figures. The contributions of convective and diffusive transport are represented by Pe number, mass transport velocity (Va ± nVa), and turnover time (T).

B High Péclet number and interstitial flow stimulate vascular network formation

Fig. 3A1 shows the first design to create a microenvironment dominated by interstitial flow (Pe > 10), such that diffusion of nutrients and waste products is negligible compared to the rate of convective transport. A high pressure gradient is induced across the cell construct by sending the top microfluidic channel through a high fluidic resistance (a long serpentine channel structure) prior to becoming the lower microfluidic channel. The simulated streamlines (Fig. 3A2) demonstrate that flow is predominantly in the transverse direction with minimal interaction between adjacent communication pores. The microfluidic channels are filled with red dye to illustrate the channel design including the jumper (Fig. 3A3, removable tubing enabling the transition from gel loading to tissue development and subsequently, tissue testing under flow. See supplement). Fluorescent dextran loaded into the top microfluidic channel highlights the direction and rate of transport (Fig. 3A4 and 3A5 1 s after loading, and Fig. 3A6 and 3A7 90 s after loading for model simulation and experimental observation, respectively). Four different ΔP conditions were applied to this design (5, 10, 15, and 20 mm H_2O), which resulted in Va = 2.3–9.0 μm s^{-1}, n = 0.56, Pe = 32–130, and T = 63–150 s. Extensive vascular formation was observed after 10 days of culture in all four conditions (Fig. 3A8 and supplement).

Alternatively, the pattern of interstitial convective flow with Pe > 10 can be longitudinal by having high pressure on the left side of the microchamber and low pressure on the right side. Routing each of the microfluidic channels through a fluidic resistance (serpentine channel) after each connecting pore created this pattern (Fig. 3B1 and 3B2). The longitudinal flow was verified experimentally using fluorescent dextran (Fig. 3B4 and 3B6, 30 min interval) and numerical simulations (Fig. 3B5 and 3B7, 13 min interval). The same four different ΔP values were also applied to this design, creating Va = 1.7–6.8 μm s^{-1}, n = 0.21, Pe = 24–97 and T = 10–40 min. Similar extensive capillary morphogenesis is observed in all four conditions (Fig. 3B8 and supplement). Since the interstitial flow path is three times longer compared to the transverse direction, the calculated turnover time T is one order of magnitude higher [10–40 min compared to ~1 min].

C Intermediate Péclet number limits vascular network formation

To create a smaller transverse pressure drop across the microchambers for creating an intermediate Pe number, the microchannel exiting the top pores can be immediately routed to connect to the bottom pores with a short length, and then to the large resistance of serpentine channels (Fig. 3C1). This creates Pe number between 0.1 and 10, where both convective and diffusive mass transport are of similar magnitude. This creates a moderate transverse pressure gradient (approximately 0.5 Pa) and interstitial convective flow (Fig. 3C2). Fig. 3C4 and 3C6 show the intensity of dextran fluorescence at 1 h and 3 h after loading in the top channel, and Fig. 3C5 and 3C7 show corresponding simulation results. The intensity from the top pores is higher and the spatial distribution is wider than from the pores on the bottom. This result is consistent with contributions from both convection and diffusion. From the top pore, convection and diffusion create net transport in the same direction (from the pore and into the microchamber); however, from the bottom pore, convection is from the microchamber and out of the pore, while diffusion is the opposite (in the direction of the concentration gradient). Three different ΔP values were applied to this design (5, 10, and 15 mmHg), creating Va = 0.03–0.1 μm s^{-1}, Pe = 0.46–1.4 and T = 18–26 h. Less developed vascular network formation occurs in all the intermediate Pe conditions (Fig. 3C8 and supplement).

D Low Péclet number and hypoxia stimulate vascular network formation

Maintaining essentially the same pressure throughout the microchamber creates a physiological hypoxic environment (Fig. 3D1). In this design, the top and bottom microchannels are formed by splitting the incoming channel such that the hydrostatic pressures on either side of the microchamber are exactly the same (Fig. 3D2). The longitudinal pressure gradient is

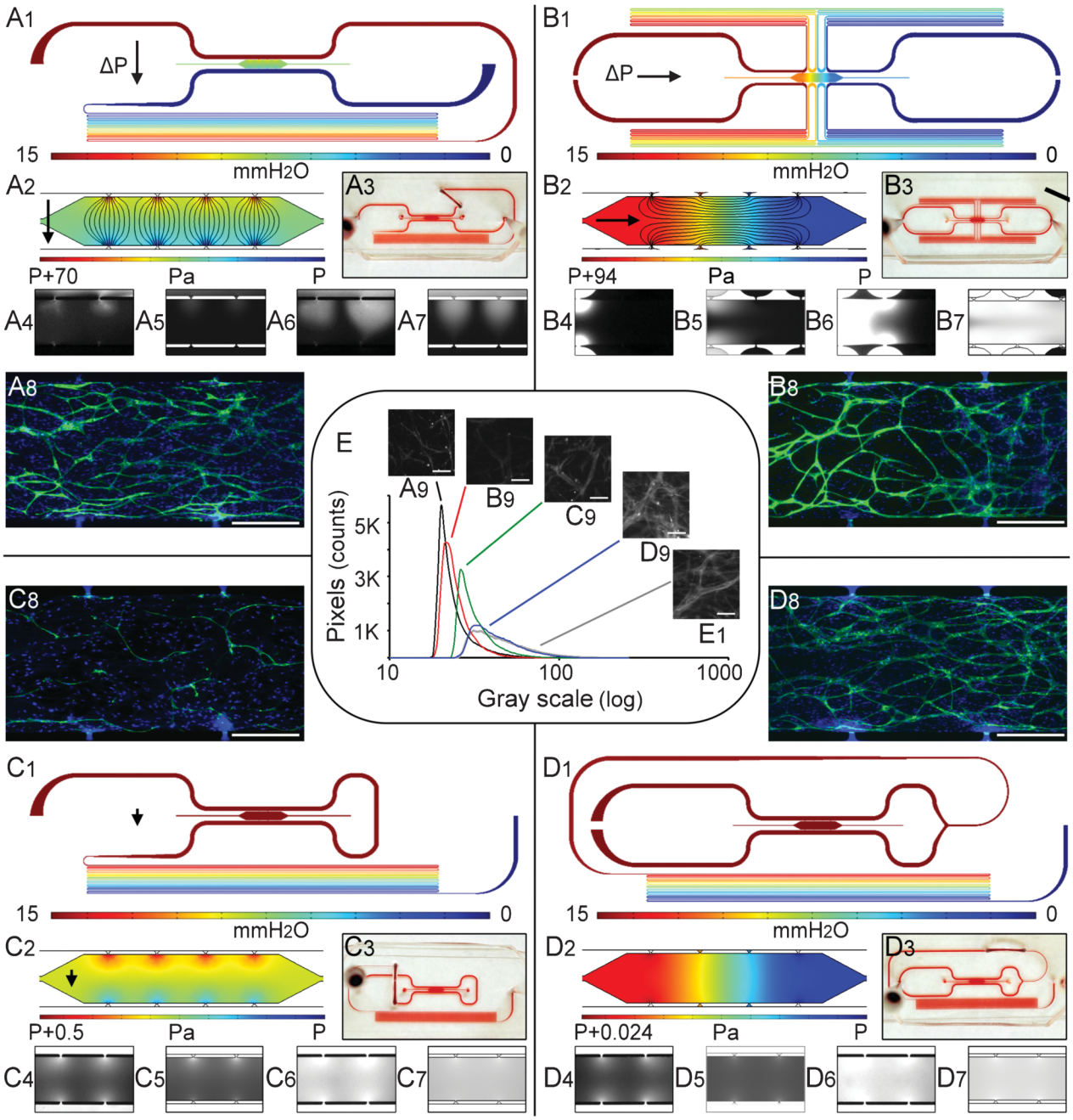

Fig. 3 Microfluidic configurations and the pressure fields of the convection-dominated microplatform for generating high interstitial flow (Pe > 10). The interstitial flow can be controlled to be aligned in the ($A_{1\text{-}3}$) transverse direction or in the ($B_{1\text{-}3}$) longitudinal direction (black lines are streamlines, and black arrows indicate the direction of interstitial flow). The microfluidic channel and microtissue compartment can also be configured to create a pressure field in which ($C_{1\text{-}3}$) convection and diffusion are of similar magnitude (Pe ~ 1), or ($D_{1\text{-}3}$) the transverse pressure gradient is zero, and the longitudinal pressure gradient is near zero and thus diffusion dominates (Pe < 0.1). Figures numbered with subscripts 4 and 6 are experimental patterns of dextran flowing into each microtissue chamber, subscripts 5 and 7 are the corresponding numerical simulation results. CD31-labeled endothelial cells after 10 days of culture demonstrate variable capillary morphogenesis at 4X (A_8, B_8, C_8, D_8), where scale bars are 500 μm. Fluorescent images of the microtissue stained with hyproxyprobeTM-1 under 5% oxygen (A_9, B_9, C_9, D_9) are compared to the positive hypoxic. control 1% oxygen (e1). (e) The histogram of hyproxyprobeTM-1 for the 5% oxygen and the 1% oxygen condition (gray line) in log scale.

very small (7.8 mPa/mm), and thus mass transport is diffusion dominated (Pe < 0.1). Experimental (Fig. 3D4 and 3D6) and model simulations (Fig. 3D5 and 3D7) of dextran fluorescent intensity at one-hour and five-hour time points, respectively, demonstrates that the distribution of dextran fluorescent intensity spreads evenly into the microchamber through all the pores, consistent with pure diffusion. Three different ΔP values were investigated in this design (5, 10, and 15 mm H_20), creating Va = 0.0004–0.0012 μm s^{-1} and Pe = 0.0056–0.017. T was independent of ΔP and equal to 33 h. Despite negligible convective interstitial transport, extensive microvascular formation is observed after 10 days of culture [Fig. 3D8 and supplement].

E Controlled microphysiological environment is verified by oxygen tension

HypoxyprobeTM-1 is used to investigate oxygen tension in the microtissue chamber. The HypoxyprobeTM-1 signal from a large area (0.435 mm by 0.331 mm) of a representative image for normoxia (5% incubator oxygen) is compared to the hypoxic control (1% incubator oxygen) (Fig. 3E1). Hypoxia is absent within the microtissue chambers dominated by interstitial flow (Pe $>$ 10, Fig. 3A9 and 3B9). The HypoxyprobeTM-1 histogram of the intermediate condition (0.1 $<$ Pe $<$ 10) is wider (evidence of hypoxia; Fig. 3C9) than in the high Pe condition, but smaller than the hypoxia control. The histogram of the HypoxyprobeTM-1 signal for the diffusion dominant microplatform (Fig. 3D, Pe $<$ 0.1) is much wider (Fig. 3D9) and indistinguishable from the hypoxic (1% oxygen) condition, consistent with significant hypoxia.

F Vasculogenic response is a function of Pe number

The influence of Pe on vasculogenesis is quantified using the total length of the microvessel network, the total number of capillary segments, and the total number of nuclei (Fig. 4A, 4B and 4C, respectively). All experimental conditions are listed, including 8 and 16 communication pore designs as well as transverse and longitudinal convective flow using different symbols. All data points were normalized to the Pe$\sim$1 group and represented by a relative ratio (R). The data clearly demonstrate a bi-phasic response in total capillary length in which high (Pe $>$ 10) and low (Pe $<$ 0.1) Pe regions produce similar vascular networks, which are significantly higher than the intermediate region (0.1 $<$ Pe $<$ 10).

Further, there was no significant increase in cell number for Pe $>$ 10 compared to Pe $<$ 0.1 (Fig. 4C). This verified that cell growth did not increase under a physiological environment with a high convective flow. This result ruled out the possibility that a hypoxic environment could be introduced at a latter stage of vessel growth at Pe $>$ 10 region and result in extensive vessel formation. To further verify the microtissue chamber was still under high convective flow for Pe $>$ 10 microplatforms at later time points, we monitored the mass transport in the developed microtissue by using the microfluidic configuration shown in Fig. 3A at day-3 and day-10. A FITC-dextran solution was flowed into the microtissue chamber from the high pressure side at ΔP = 15 mm H_2O. The flow was nearly the same on day-3, and decreased 11%–33% on day-10. However, the calculated Pe numbers were still $>$10. The decrease of flow was due to extensive vessel growth next to the pores, and the dextran (70 kDa) used was not permeable to vessels.

G 3-D Microtissue with matured microvasculature

Since the presented platform could provide a physiological environment for stimulating vasculogenesis and developing the microvasculature, the capability to grow a microtissue with a more mature microvasculature was investigated. Microfluidic platforms dominated by interstitial flow in transverse (Fig. 3A) and longitudinal directions (Fig. 3B) were chosen for this study and microtissues were cultured for 21 days. Fig. 5A and 5B are the micrographs of the transverse and longitudinal microvasculature, respectively. Fig. 5C and 5D are the corresponding cross-sectional confocal images. Well-defined lumens with increased diameters were found. The average (SD) diameter was 28.0 (12.7) μm (Fig. 5C) and 33.9 (9.88) μm (Fig. 5D), respectively, which are larger than the microvessels observed at day-10, where the average (SD) diameter were 19.3 (4.29) μm (Fig. 3A8) and 21.8 (6.40) μm (Fig. 3B8).

Discussion

A Impact of Péclet number on vasculogenesis

The low Pe condition in our system was associated with a higher level of hypoxia demonstrating that oxygen transport was diffusion-limited under this condition. It is well-documented that hypoxia stimulates new blood vessel formation *in vivo*,[31,32] and this has also been recapitulated with *in vitro* models,[33] The mechanisms are well-understood, and include stabilization, followed by translocation of the HIF-α transcriptional complex from the cytoplasm to the nucleus where it binds to HIF responsive elements (HREs) on DNA and initiates the transcription of numerous pro-survival genes including VEGF.[32] If hypoxia is too severe, cells will undergo apoptosis; thus, the creation of robust vessel networks in our system at low Pe suggests an appropriate level of hypoxic stress to induce a pro-survival response.

Our observation that only high Pe stimulate vasculogenesis, while neither high (Pe $>$ 10, convective velocity 1.7–11 μm s^{-1}) nor intermediate (0.1 $<$ Pe $<$ 10, convective velocity 0.025–0.1

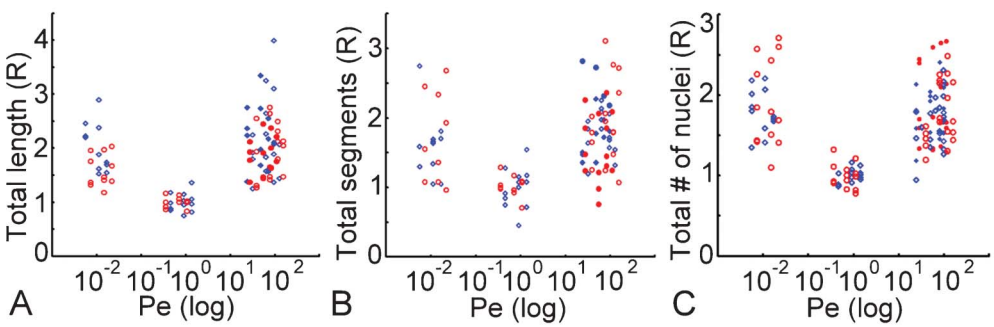

Fig. 4 Comparison of (A) total capillary length, (B) total capillary segments, and (C) total number of nuclei as a function of the Pe. Blue diamonds and red circles are data from platforms with 8 and 16 pores, respectively. At Pe $>$ 10, filled and open symbols correspond to transverse and longitudinal interstitial flow, respectively. The *x*-axes are in log scale.

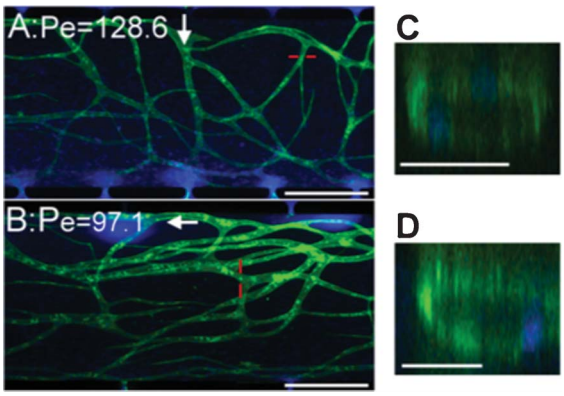

Fig. 5 (A) and (B) are micrographs of microvasculature developed for 21 days by using interstitial flow dominant microplatform shown in Fig. 2A [transversely] and Fig. 2B [longitudinally]. (C) and (D) are cross-sectional confocal images of developed microvessels of (A) and (B) at red lines. The scale bars are 500 μm (A) and (B), and 40 μm for confocal images (C) and (D).

μm s^{-1}) Pe conditions were associated with hypoxia, suggests that interstitial flow alone can stimulate vessel formation. While we did not pursue the specific mechanism in this study, this observation is consistent with previous reports demonstrating that high interstitial fluid flow (6.3 μm s^{-1}) can stimulate the transition and proliferation of fibroblasts to myofibroblasts, the latter of which secretes high levels of pro-angiogenic growth factors such as TGF-β1[34] and VEGF.[35] The physiological benefit of this response is not well-understood. However, normal interstitial velocity ranges from 0.1–1.0 μm s^{-1}.[21] In our system this corresponds to approximately $1.4 < Pe < 15$, or a range that falls between the intermediate flow range which limits vasculogenesis, and the high flow range which stimulates vasculogenesis. This observation suggests that interstitial flow may be used *in vivo* to regulate vessel formation. There is significant evidence in the literature to suggest that the enhanced metabolic demand in conditions such as exercise[36] or cancer[37–39] are associated with higher interstitial flow as well as with new vessel formation. Thus, the intermediate Pe condition did not stimulate vessel formation likely because oxygen was not low enough to induce a hypoxic pro-survival response, and the interstitial flow velocity was not high enough to stimulate vessel formation. An indirect conclusion from this observation is that the interstitial flow and the hypoxia mechanism inducing vasculogenesis are independent of each other.

B Potential applications and utility of platform

While our studies have demonstrated the utility of our platform to investigate the relative roles of diffusion and interstitial convection on vasculogenesis, the platform has broader applications in the fields of tissue engineering, microphysiological system modeling, wound healing, personalized medicine, cancer, drug discovery, and cell biology. Furthermore, our study varies not only the interstitial flow itself but also the ratio between interstitial flow and diffusion based transport (*i.e.* Pe) and has revealed new insights on the how interstitial flow and hypoxia are independent control parameters for vasculogenesis. Each of these fields has significant hurdles limiting their development, and although some are specific, many are more general that our platform can address. For example, controlling cell behavior (migration, differentiation, replication) is fundamental to creating new tissues for implant or *in vitro* models of tissues for drug discovery. Mechanical forces such as interstitial flow and the delivery of nutrients by convection and diffusion are potent forces that impact cell behavior, as has recently been demonstrated in the migration of cancer cells.[40,41] Second, tissue repair, disease, and infection requires a transportation system for delivery of nutrients and immune cells, and removal of waste products that is substantially different from normal or healthy tissue. Third, the capability to program the direction of interstitial flow in a controlled microenvironment can also become a unique model system. It provides a controlled physiological microenvironment in the microchamber to study the correlation between cellular/tissue behavior and the direction of interstitial flow. This type of relationship has been demonstrated *in vivo* as the orientation of a lymphatic capillary network is primarily in the direction of interstitial flow,[42] and the lymphatic endothelial cells tend to align with interstitial flow in an *in vitro* model.[12] Advancing our understanding of these phenomena will be facilitated by a high-throughput microfluidic platform with control over a wide range of interstitial flow and diffusion. Finally, more advanced microphysiological systems that attempt to integrate a plurality of organ systems will need a platform that includes control over convective and diffusive transport of nutrients and waste.

Conclusions

We present a universal microfluidic platform that provides a simple and straightforward means to create microphysiological environments with precise control over the direction and magnitude of mass transport. The utility of our platform to investigate new biological questions is demonstrated by quantitatively determining the impact of Pe on vasculogenesis. Both experimental and simulation results verify that the relative contributions of convective and diffusive mass transport can be carefully controlled over a wide range, and significantly impact vessel formation. By using a long microfluidic channel, large media reservoirs, multiple communication pores, and necking channels, the microfluidic platform demonstrates that high interstitial flow and near zero (hypoxia) interstitial flow can independently stimulate vasculogenesis. When convective and diffusive transports are similar in magnitude ($0.1 < Pe < 10$), an unfavorable environment for vasculogenesis is created. The results of our platform are consistent with the physiological observation that little blood vessel growth occurs in normal healthy tissue where the Pe in the interstitial space ranges from 1 to 15. However, disease or altered physiological states (*e.g.*, tumor, wound healing, exercise) can drastically impact Pe resulting in a microenvironment conducive for new vessel growth to meet metabolic demands.

Acknowledgements

The authors acknowledge the continuous support by Dr Tatiana Krasieva for confocal images. This research was supported by National Institutes of Health RC1 ES018361-01.

References

1 D. E. Discher, P. Janmey and Y-l Wang, Tissue cells feel and respond to the stiffness of their substrate, *Science*, 2005, **310**, 1139–1143.
2 F. Rosso, A. Giordano, M. Barbarisi and A. Barbarisi, From cell–ECM interactions to tissue engineering, *J. Cell. Physiol.*, 2004, **199**, 174–180.
3 F. Pampaloni, E. G. Reynaud and E. H. K. Stelzer, The third dimension bridges the gap between cell culture and live tissue, *Nat. Rev. Mol. Cell Biol.*, 2007, **8**, 839–845.
4 J. A. Pedersen, S. Lichter and M. A. Swartz, Cells in 3D matrices under interstitial flow: Effects of extracellular matrix alignment on cell shear stress and drag forces, *J. Biomech.*, 2010, **43**, 900–905.
5 J. M. Tarbell and Z.-D. Shi, Effect of the glycocalyx layer on transmission of interstitial flow shear stress to embedded cells, *Biomech. Model. Mechanobiol.*, 2012, DOI: 10.1007/s10237-012-0385-8.
6 P. A. Galie, M. W. Russell, M. V. Westfall and J. P. Stegemann, Interstitial fluid flow and cyclic strain differentially regulate cardiac fibroblast activation via AT1R and TGF-β1, *Exp. Cell Res.*, 2012, **318**, 75–84.
7 Z.-D. Shi, H. Wang and J. M. Tarbell, Heparan sulfate proteoglycans mediate interstitial flow mechanotransduction regulating MMP-13 expression and cell motility via FAK-ERK in 3D collagen, *PLoS One*, 2011, **6**, e15956.
8 W. J. Polacheck, J. L. Charest and R. D. Kamm, Interstitial flow influences direction of tumor cell migration through competing mechanisms, *Proc. Natl. Acad. Sci. U. S. A.*, 2011, **108**, 11115–11120.
9 J. D. Shields, M. E. Fleury, C. Yong, A. A. Tomei, G. J. Randolph and M. A. Swartz, Autologous chemotaxis as a mechanism of tumor cell homing to lymphatics via interstitial flow and autocrine CCR7 signaling, *Cancer Cell*, 2007, **11**, 526–538.
10 C. Ruhrberg, H. Gerhardt, M. Golding, R. Watson, S. Ioannidou, H. Fujisawa, C. Betsholtz and D. T. Shima, Spatially restricted patterning cues provided by heparin-binding VEGF-A control blood vessel branching morphogenesis, *Genes Dev.*, 2002, **16**, 2684–2698.
11 C.-L. E. Helm, A. Zisch and M. A. Swartz, Engineered blood and lymphatic capillaries in 3-D VEGF-fibrin-collagen matrices with interstitial flow, *Biotechnol. Bioeng.*, 2007, **96**, 167–176.
12 C. P. Ng, C.-L. E. Helm and M. A. Swartz, Interstitial flow differentially stimulates blood and lymphatic endothelial cell morphogenesis *in vitro*, *Microvasc. Res.*, 2004, **68**, 258–264.
13 R. Sudo, S. Chung, I. K. Zervantonakis, V. Vickerman, Y. Toshimitsu, L. G. Griffith and D. K. Roger, Transport-mediated angiogenesis in 3D epithelial coculture, *FASEB J.*, 2009, **23**, 2155–2164.
14 Y. Shin, J. S. Jeon, S. Han, G. S. Jung, S. Shin, S. H. Lee, R. Sudo, R. D. Kamm and S. Chung, In vitro 3D collective sprouting angiogenesis under orchestrated ANG-1 and VEGF gradients, *Lab Chip*, 2011, **11**, 2175–2181.
15 R. H. Adams and K. Alitalo, Molecular regulation of angiogenesis and lymphangiogenesis, *Nat. Rev. Mol. Cell Biol.*, 2007, **8**, 464–478.
16 C.-L. E. Helm, M. E. Fleury, A. H. Zisch, F. Boschetti and M. A. Swartz, Synergy between interstitial flow and VEGF directs capillary morphogenesis in vitro through a gradient amplification mechanism, *Proc. Natl. Acad. Sci. U. S. A.*, 2005, **102**, 15779–15784.
17 C. E. Semino, R. D. Kamm and D. A. Lauffenburger, Autocrine EGF receptor activation mediates endothelial cell migration and vascular morphogenesis induced by VEGF under interstitial flow, *Exp. Cell Res.*, 2006, **312**, 289–298.
18 A. Shamloo and S. C. Heilshorn, Matrix density mediates polarization and lumen formation of endothelial sprouts in VEGF gradients, *Lab Chip*, 2010, **10**, 3061–3068.
19 V. R. Hernández, E. Genové, L. Alvarez, S. Borrós, R. D. Kamm, D. Lauffenburger and C. E. Semino, Interstitial fluid flow intensity modulates endothelial sprouting in restricted Src-activated cell clusters during capillary morphogenesis, *Tissue Eng. A*, 2009, **15**, 175–185.
20 C. M. Ghajar, X. Chen, J. W. Harris, V. Suresh, C. C. Hughes, N. L. Jeon, A. J. Putnam and S. C. George, The effect of matrix density on the regulation of 3-D capillary morphogenesis, *Biophys. J.*, 2008, **94**, 1930–1941.
21 C. Bonvin, J. Overney, A. C. Shieh, J. B. Dixon and M. A. Swartz, A multichamber fluidic device for 3D cultures under interstitial flow with live imaging: development, characterization, and applications, *Biotechnol. Bioeng.*, 2010, **105**, 982–991.
22 A. Schmidt, K. Brixius and W. Bloch, Endothelial precursor cell migration during vasculogenesis, *Circ. Res.*, 2007, **101**, 125–136.
23 A. C. Shieh, H. A. Rozansky, B. Hinz and A. S. Melody, Tumor cell invasion is promoted by interstitial flow-induced matrix priming by stromal fibroblasts, *Cancer Res.*, 2010, **71**, 790–800.
24 S. Chung, R. Sudo, P. J. Mack, C. R. Wan, V. Vickerman and R. D. Kamm, Cell migration into scaffolds under co-culture conditions in a microfluidic platform, *Lab Chip*, 2009, **9**, 269–275.
25 A. D. Stroock and C. Fischbach, Microfluidic culture models of tumor angiogenesis, *Tissue Eng. A*, 2010, **16**, 2143–2146.
26 K. W. Oh, K. Lee, B. Ahn and E. P. Furlani, Design of pressure-driven microfluidic networks using electric circuit analogy, *Lab Chip*, 2012, **12**, 515–545.
27 X. Chen, A. S. Aledia, S. A. Popson, L. Him, C. C. Hughes and S. C. George, Rapid anastomosis of endothelial progenitor cell–derived vessels with host vasculature is promoted by a high density of cotransplanted fibroblasts, *Tissue Eng. A*, 2010, **16**, 585–594.
28 C. K. Griffith, C. Miller, R. C. Sainson, J. W. Calvert, N. L. Jeon, C. C. Hughes and S. C. George, Diffusion limits of an in vitro thick prevascularized tissue, *Tissue Eng.*, 2005, **11**, 257–266.
29 H. Cho, H.-Y. Kim, J. Y. Kang and T. S. Kim, How the capillary burst microvalve works, *J. Colloid Interface Sci.*, 2007, **306**, 379–385.
30 M. E. Cox and B. Dunn, Oxygen diffusion in poly(dimethyl siloxane) using fluorescence quenching. I. measurement technique and analysis, *J. Polym. Sci., Part A: Polym. Chem.*, 1986, **24**, 621–636.
31 K. S. Choi, M. K. Bae, J. W. Jeong, H. E. Moon and K. W. Kim, Hypoxia-induced angiogenesis during carcinogenesis, *J. Biochem. Mol. Biol.*, 2003, **36**, 120–127.
32 C. W. Pugh and R. J. Ratcliffe, Regulation of angiogenesis by hypoxia: role of the HIF system, *Nat. Med.*, 2003, **9**, 677–684.
33 C. K. Griffith and S. C. George, The effect of hypoxia on in vitro prevascularization of a thick soft tissue, *Tissue Eng. A*, 2009, **15**, 2423–2434.
34 C. P. Ng, B. Hinz and M. A. Swartz, Interstitial fluid flow induces myofibroblast differentiation and collagen alignment *in vitro*, *J. Cell Sci.*, 2005, **118**, 4731–4739.
35 V. Chintalgattu, D. M. Nair and L. C. Katwa, Cardiac myofibroblasts: a novel source of vascular endothelial growth factor (VEGF) and its receptors Flt-1 and KDR, *J. Mol. Cell. Cardiol.*, 2003, **35**(3), 277–286.
36 E. M. Knott, J. D. Tune, S. T. Stoll and H. F. Downey, Increased lymphatic flow in the thoracic duct during manipulative intervention, *J. Am. Osteopath Assoc.*, 2005, **105**(10), 447–456.
37 T. P. Butler, F. H. Grantham and P. M. Gullino, Bulk transfer of fluid in the interstitial compartment of mammary tumors, *Cancer Res.*, 1975, **35**, 3084–3088.
38 A. Ruddell, M. I. Harrell, S. Minoshima, K. R. Maravilla, B. M. Iritani, S. W. White and S. C. Partridge, Dynamic contrast-enhanced magnetic resonance imaging of tumor-induced lymph flow, *Neoplasia*, 2008, **10**, 706–713.
39 A. C. Shieh, Biomechanical forces shape the tumor microenvironment, *Ann. Biomed. Eng.*, 2011, **39**(5), 1379–1389.
40 W. J. Polacheck, J. L. Charest and R. D. Kamm, Interstitial flow influences direction of tumor cell migration through competing mechanisms, *Proc. Natl. Acad. Sci. U. S. A.*, 2011, **108**, 11115–11120.
41 U. Haessler, J. C. M. Teo, D. Foretay, P. Renaud and M. A. Swartz, Migration dynamics of breast cancer cells in a tunable 3D interstitial flow chamber, *Integr. Biol.*, 2012, **4**, 401–409.
42 K. C. Boardman and M. A. Swartz, Interstitial Flow as a Guide for Lymphangiogenesis, *Circ. Res.*, 2003, **92**, 801–808.